Hindawi
Advances in Civil Engineering
Volume 2020, Article ID 6678620, 9 pages
https://doi.org/10.1155/2020/6678620

*Research Article*

# Management and Fractal Analysis of Desiccation Cracks of Soils with Acid Contamination

**Xin Wang**[1], **Binbin Yang**[1,2], **Lichuang Jin**[1,3], **Zepeng Zhang**[2] and **Xinyang Xu**[2]

[1]*School of Economics and Management, China University of Mining and Technology, Xuzhou, Jiangsu 221008, China*
[2]*School of Civil Engineering, Xuchang University, Xuchang, Henan 461000, China*
[3]*College of Geoscience and Surveying Engineering, China University of Mining and Technology (Beijing), Beijing 100083, China*

Correspondence should be addressed to Binbin Yang; yangbinbin@cumt.edu.cn and Lichuang Jin; jlc@cumt.edu.cn

Received 11 November 2020; Revised 20 November 2020; Accepted 26 November 2020; Published 7 December 2020

Academic Editor: Bingxiang Yuan



Soil pollution due to acid contamination changes the chemical state of the soil and affects the water evaporation and desiccation cracking characteristics of the soil. The contamination of soils is becoming a serious problem due to increases in manufacturing, construction, and industrial activities, especially in and around urban areas. Soil pollution has become a global issue with serious and harmful impacts on the environment. The purpose of this paper is to present a study on the evaporation characteristics of soil contaminated with different acid concentrations. The result indicates that water evaporation in soils can be divided into three stages: the steady rate of evaporation, deceleration of evaporation, and residual evaporation stages. With increases in acid concentration, there is critical water content at which the rate of evaporation starts to decrease with increase in the duration of evaporation. Surface crack development in soils with different acid concentrations can be divided into three stages: initial cracking, crack development, and crack stabilization. When the acid concentration is higher than 0.4 mol/L, the initial cracking and stabilization stages disappear, and cracks continue to develop until they become stable.

## 1. Introduction

Rapid industrial and urban developments have resulted in serious soil pollution in many parts of the world [1–3]. The northwestern part of China has a fragile ecological environment which is more prone to be affected by rapid industrial development. As such, soil pollution due to acid from the leakage of chemical waste and acid rain has become a serious problem there [4]. Pollutants in the soil can be directly or indirectly absorbed by surface vegetation. With the advancement of urbanization in the western regions of China, land resources have become particularly scarce, and the management of contaminated soil has therefore become an important issue in geotechnical and geo-environmental engineering [5–7]. Aside from soil contamination, industrial activities also cause acid rain from the release of sulfur dioxide and nitrogen oxide (acid forming compounds) into the environment when fossil fuels are used. Acid rain affects the environment in many ways. Such as does this acidic precipitation directly damage the environment and changes the chemistry of the soil which affects vegetation growth and biological habitats. Moreover, it is difficult to maintain a sustainable ecosystem with acid rain [8, 9]. The impact of soil pollution due to acidic precipitation on terrestrial ecosystems is a major environmental issue which can be found in many countries. The acidic pollution of soil affects the effectiveness, mobility, and activity of biological organisms in the soil, thus resulting in the substantial release of heavy metals in the soil due to the presence of hydrogen, calcium, magnesium, and ammonium ions ($H^+$, $Ca^{2+}$, $Mg^{2+}$, and $NH^{4+}$). Acid pollution has become one of the important reasons for the acidification of the environment. This has resulted in the increased mobility of cadmium (Cd) ions and its toxicity to plants even though the mobility of Cd ions in soil is lower at higher pH values [10].

The problem of soil contamination is further exacerbated with soil shrinkage and cracking, which are complex processes that have important effects on the properties of soil

and result in various engineering problems [11]. The cracking of the clay barrier and clay overburden materials in landfills will facilitate leachate migration which poses the threat of pollution to groundwater and the geological environment [12, 13]. Soil cracking is also a key factor that reduces the stability of slopes in expansive soil since the surface cracks increase rainwater infiltration thus resulting in a significant reduction in the safety factor of the slopes and leading to landslide hazards [14, 15]. Soil cracking reduces the bearing capacity of soil and increases its compressibility which results in cracking and failure of building foundations. Cracking also increases the permeability of soil which adversely affects groundwater flow and plant growth. With global warming and the occurrence of more extreme climatic conditions, especially in arid land, soil cracking will cause even more serious engineering problems in the future.

The problem of soil cracking has been well studied in the literature. For instance, to study crack development in soils, Hallett and Newson performed a deep notch bending test to evaluate the crack tip opening angle (CTOA) in clay. Soil cracking under a wet plastic state was analyzed by using a new elastic-plastic fracture mechanics model [16]. Drying experiments of clay indicated that with an increase in the particle size of the soil, the density of the cracks decreases and the length of the cracks is increased [17]. Ground penetrating radar (GPR) has been used to detect the formation of soil cracking during drying. It has been found that GPR can detect cracks with a width of 1 to 2 mm which improves understanding of soil cracking [18]. Wang et al. examined the dynamic cracking phenomenon of soil through wetting-drying (W-D) cyclic tests which showed the differences in the crack morphology between cracking and dissolution. They also examined the degree of repeatability of their test results on soil cracking which helps us to quantify the shrinkage/expansion process and water migration in soils [19].

Many previous studies have also explored the mechanism of drying and cracking in soils. However, few have considered the effects of acid contamination. The pore structure, bulk density and water retention capabilities of soil are changed due to changes in soil chemistry as a result of acid contamination. This also affects water evaporation and desiccation crack development in soil. As such, the main purpose of this study is to investigate the water retention capacity and crack development of acidic soil. The fractal dimension method is used to analyze desiccation crack development. The crack characteristics and rate of evaporation of acidic soil with different acid concentrations are studied. The mechanism of crack development and its practical implications on soil are examined.

## 2. Laboratory Experiments and Test Materials

*2.1. Test Materials.* To understand crack development in soils, a laboratory testing program is carried out in this study. The soil used in the test was taken from Yuzhou City in Henan Province, China. The samples were obtained at a depth between 0.5 m and 1.0 m in a weakly acidic groundwater environment. Yuzhou City is in the warm temperate region with a monsoon climate (Figure 1) and therefore has many warm days, abundant rainfall, sufficient sunlight, and many long frost-free days during the year. Due to its continental climate with monsoonal rains, Yuzhou City faces many weather-related challenges such as droughts, waterlogging, strong winds, and hail. The average annual temperature lies between 13°C and 16°C. The average annual precipitation is about 650 mm, and the average annual wind speed is about 2.5 m/s.

After the soil samples were obtained from the field, they were air-dried outdoors and broken into pieces with the use of a wooden hammer. The soil was screened through a 2 mm sieve to remove large lumps and large soil particles. The soil samples were then stored in a sealed bucket for testing. The physical and mechanical properties of the soil are summarized in Table 1. In order to simulate the effect of acid pollution, concentrated hydrochloric acid (HCl) with an initial mass fraction of 36.5% was added to the soil.

*2.2. Laboratory Experiments.* In preparing the soil samples for testing, water was added to the soil and stirred thoroughly and evenly. An appropriate amount of HCl was added to produce saturated slurry with an initial water content close to 100%. The acid concentrations (ACs) of the samples were equal to 0.1, 0.2, 0.3, and 0.4 mol/L. The slurry samples were placed in a sealed rectangular parallelepiped glass container of $25 \times 25 \times 4$ cm in size and stored in a constant temperature and humidity chamber for 10 days.

Distilled water was added to some of the samples to be used in the control group. The control group samples were also placed in a constant temperature and humidity chamber for 10 days. All of the samples were stored for 10 days to provide sufficient time for the acid to react with the soil to produce a homogeneous sample in order to improve the repeatability of the test results. A total of 5 sets of samples with different acid concentrations were prepared for testing with 3 soil samples for each set so that the each test could be conducted three times. The test parameters are summarized in Table 2.

The samples together with the electronic balance were placed in a drying chamber at a constant temperature, and the samples were dried at a temperature of 25°C with a relative humidity of 40%, as shown in Figure 2. During drying, the changes in the weight of the samples were recorded by using a computer, which were used to calculate the evaporation rate and the average water content of the samples. The evaporation rate per unit area of the soil surface, $E_a$, can be determined from

$$E_a = \frac{\Delta m}{S \bullet t}, \tag{1}$$

where $\triangle m$ is the change in mass of the soil sample which is equal to the mass of the water evaporated, $S$ is the surface area of the soil sample, and $t$ is the elapsed time of evaporation.

*2.3. Image Processing of Surface Crack Photos.* In order to study crack development during drying, a camera was used

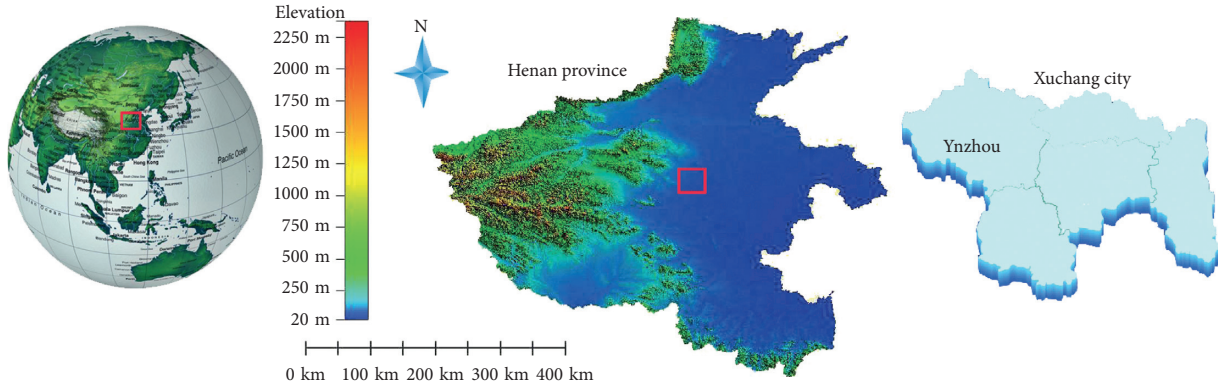


Figure 1: Location of Yuzhou city.

Table 1: Physical and mechanical properties of clay soil.

| Density ($g \cdot cm^{-3}$) | Liquid limit (%) | Plastic limit (%) | Plasticity index | Cohesion (kPa) | Internal friction angle (°) | Coefficient of compressibility ($MPa^{-1}$) | Modulus of compressibility (MPa) |
|---|---|---|---|---|---|---|---|
| 1.88 | 60.34 | 37.71 | 22.63 | 58.13 | 23.31 | 0.223 | 9.094 |

Table 2: Parameters of soil samples.

| Sample number | Concentration of hydrochloric acid ($mol \cdot L^{-1}$) | Number of samples | Thickness of sample (mm) |
|---|---|---|---|
| 1 | 0 | 3 | 5 |
| 2 | 0.1 | 3 | 5 |
| 3 | 0.2 | 3 | 5 |
| 4 | 0.3 | 3 | 5 |
| 5 | 0.4 | 3 | 5 |

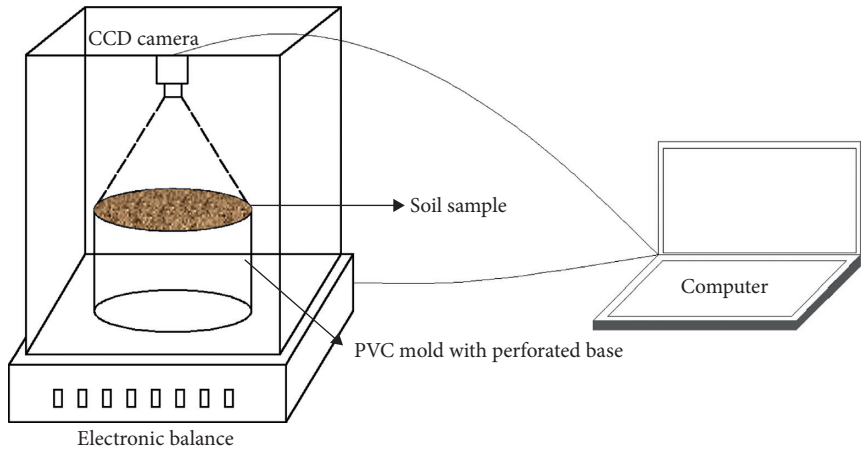


Figure 2: Schematic of laboratory setup.

to capture digital images of the soil surface (Figure 2). Before a quantitative analysis of the images can be carried out, the images had to be processed to eliminate digital noise and interference in order to highlight the cracks. There are digital noises in the image data, and the edge of the crack may not be clear. To improve the image quality, the median filtering method was used to remove image noise. Figure 3 shows the crack image after undergoing median filtering several times. The color images contain a large amount of data which makes it inefficient to extract crack information from the images. The color images were therefore converted into grayscale images. Grayscale is usually divided into 256 shades of gray which are represented by a number from 0 to 255. The darkest gray is black which is represented by the number 0, while the brightest gray is white which is represented by the number 255. A gradual transition from black to white is represented by the remaining numbers from 1 to 254. Using the

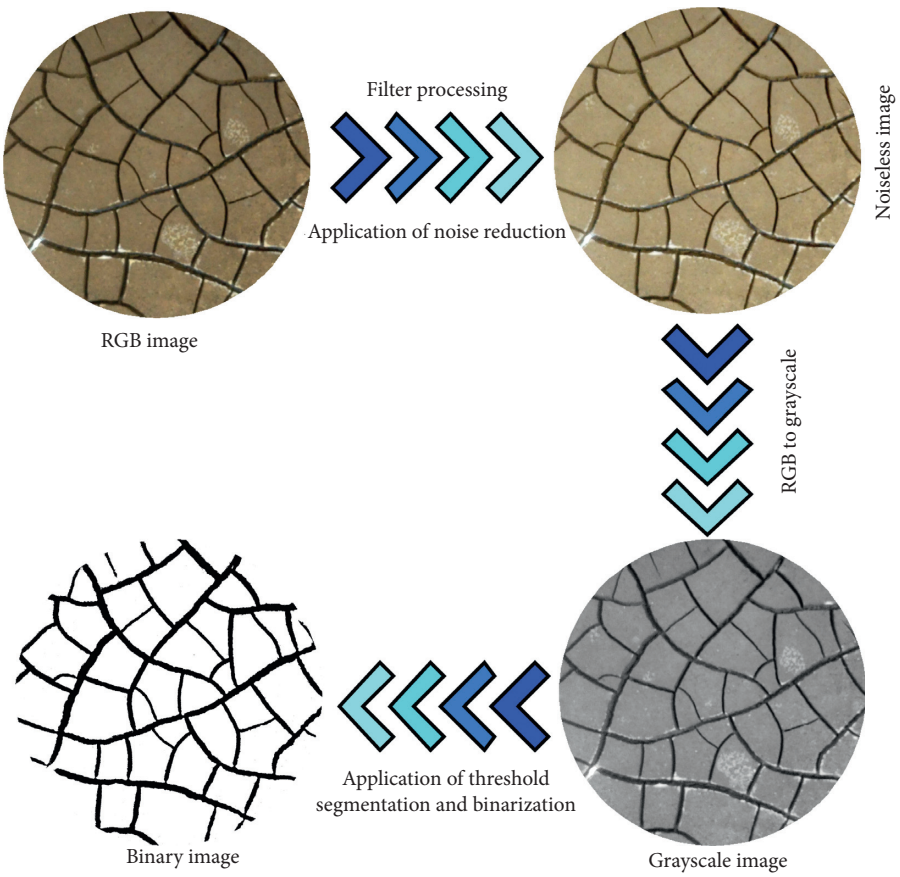


Figure 3: Processing of soil sample images.

grayscale, only one number is used to represent the color for each pixel. A two-dimensional matrix can be used to represent an image. To convert the color images to grayscale, the following equation is used:

$$G = 0.40R + 0.40G + 0.20B, \tag{2}$$

where $G$ is the grayscale with a value from 0 to 255 and $R$, $G$, and $B$ represent the color scale, with a value from 0 to 255, for red, green, and blue hues, respectively.

The effect of converting a color image into a grayscale image is shown in Figure 3. The crack appears to be clearer after the color image is converted to grayscale. Next, the threshold segmentation method is used to binarize the image to further distinguish the cracks from the rest of the soil surface. The method examines the differences in grayscale between the target object, in this case the cracks, and the background of the object—the uncracked soil surface. The image is regarded as a combination of the different gray scales in the target and background. A grayscale threshold value is used to distinguish between the target object and its background. If the grayscale of a pixel exceeds this threshold, it is considered to be the target object. Otherwise, it belongs to the background. Let the original pixel have a grayscale value of $f(x, y)$ with a threshold $T_h$, and then the binarization pixel value $g(x, y)$ is calculated from

$$g(x, y) = \begin{cases} 1, & f(x, y) \geq T_h, \\ 0, & f(x, y) < T_h. \end{cases} \tag{3}$$

As shown in equation (3), the selection of an appropriate threshold value is very important in the image binarization process. First, the initial threshold $T_h$ is determined from the grayscale histogram. The image is then divided into two parts, $R_1$ and $R_2$. Then the average gray levels $\mu_1$ and $\mu_2$ of the regions $R_1$ and $R_2$ are calculated. A new segmentation threshold $T = (\mu 1 + \mu 2)/2$ is calculated. The process is repeated until there are no changes in the threshold. Figure 3 shows that the background of the image is completely white, leaving only the cracked area black.

After processing the images and highlighting the cracks on the soil surface, it is necessary to represent the cracks with a measure/parameter so that the development of cracking can be analyzed quantitatively. Fractal analysis with the use of fractal dimension is a parameter that can be used to describe an irregular system quantitatively. Consider a one-dimensional problem of a line. Let the length of the continuous line segment be $x$, which is subdivided into $N = b$ equal segments. Each segment is proportional to the entire line but reduced. This proportion of the line segment is called similarity which is represented by the similarity ratio $r$, where $r = 1/b = 1/n$. For a two-dimensional problem, the domain can be subdivided into $N = b^2$ squares, which are

similar to the entire two-dimensional domain. Each subdomain can be represented by a coordinate $(x, y)$ such that

$$(k-1)\frac{X}{b} \le x < \frac{kX}{b} \quad (k = 1, 2, \ldots, b),$$
$$(h-1)\frac{Y}{b} \le y < \frac{kY}{b} \quad (k = 1, 2, \ldots, b). \tag{4}$$

The similarity ratio is equal to

$$r(N) = \frac{1}{b} = \frac{1}{N^{(1/2)}}. \tag{5}$$

For a $D$-dimensional domain, the similarity ratio is equal to

$$r(N) = \frac{1}{N^{(1/D)}}, \tag{6}$$

and therefore,

$$Nr^{D_s} = 1,$$
$$\log r(N) = \log\left(\frac{1}{N^{(1/D_s)}}\right) = -\frac{\log N}{D_s}, \tag{7}$$
$$D_s = -\frac{\log N}{\log r(N)} = \frac{\log N}{\log(1/r)}.$$

## 3. Laboratory Test Results

*3.1. Evaporation Process of Soil Subjected to Acid Contamination.* The evaporation of water in soils is the process of water entering the atmosphere from the soil surface which results in a decrease in the water content and gradual drying of the soil surface. As shown in Figure 4, the evaporation process with different acid concentrations in the soil can be divided into three stages: the steady rate of evaporation, deceleration of evaporation, and residual evaporation stages.

During the stage where there is a steady rate of evaporation, the soil is completely saturated and the decrease in water content at the soil surface due to evaporation is completely replenished by water transported by capillary action. Therefore, evaporation is steady. Figure 4 shows the average rate of evaporation at this stage, which is about 0.2 g/(cm$^2$·min). The evaporation force is greater than or close to the molecular force of the water at the soil surface under the immediate adjacent ambient conditions. The rate of evaporation is only affected by the ambient conditions such as temperature and humidity. For different acid concentrations 0, 0.1, 0.2, 0.3, and 0.4 mol/L, the water content in the soil is reduced to 35.63%, 35.2%, 34.85%, 34.00%, and 29.01%, respectively. With increases in the acid concentration, the rate of evaporation decreases with an increase in time. As the water content in the soil decreases, the flow of water from the bottom to the top of the sample is not sufficient enough to maintain a constant rate of evaporation, and therefore, the rate of evaporation begins to decline, and the first stage of the evaporation is completed.

In the subsequent stage where there is deceleration of evaporation, the water content in the soil continuously decreases with time, and the rate of evaporation also continues to decrease. In this stage, the water content in the soil gradually becomes the controlling factor for the rate of evaporation, while the ambient conditions play a less important role. This stage will continue until the soil surface becomes dry. The test results show that the duration of this stage decreases with increases in acid concentration.

After this is the stage where there is residual evaporation. The soil surface and the soil are quite dry, and there is no, or insufficient, water in the soil that can be transported to the surface. This results in the termination of surface evaporation. At this time, heat exchange between the soil and water takes place, and water in the soil vaporizes and escapes through the dry surface layer by molecular diffusion. The rate of vaporization of water is mainly controlled by the water content of the soil below the surface layer and the gradient of the vapor pressure in the soil. The rate of vaporization is, in general, extremely slow. As drying continues downward, a thick hard soil layer is formed on the upper part of the soil surface. Evaporation is greatly reduced since the water molecules have to go through a thicker and thicker dry layer of soil. In this stage, evaporation is mainly controlled by the characteristics of the soil layer. When the thickness of the dry layer of soil reaches a certain value, evaporation becomes constant. At this time, the water content of the soil surface is equal to the residual water content. Therefore at this stage, the amount of acid concentration has no significant effect on the rate of evaporation.

*3.2. Desiccation Cracks on Soil Surface with Different Concentrations of Acid.* Soil, in its natural state, is in the form of a porous medium. When saturated, its pores are filled with water. As shown in Figures 5 and 6, water in the soil decreases to a certain amount before surface cracks begin to appear. There are significant differences in the crack development for different acid concentrations. During drying, the decrease in the water content leads to suction and shrinkage of the soil and the development of tensile stresses. When the tensile stress exceeds the tensile strength of the material, fractures develop. Facture development can be measured by fractal dimensions. As shown in Figures 5 and 6, the development of cracks in the soil according to the fractal dimensions with different acid concentrations can be divided into three stages: Stage I is the initial stage of cracking, Stage II is the crack development stage, and Stage III is the crack stabilization

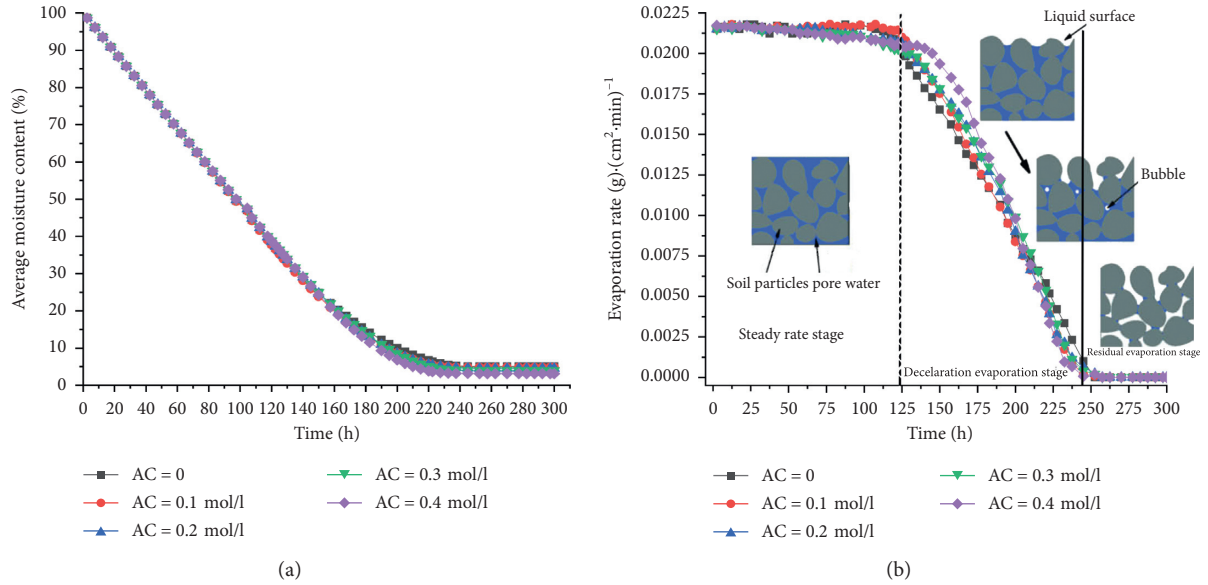


FIGURE 4: Drying time variations: (a) average moisture content of contaminated samples with different acid concentrations vs. time, (b) rate of evaporation of contaminated samples with different acid concentrations vs. time.

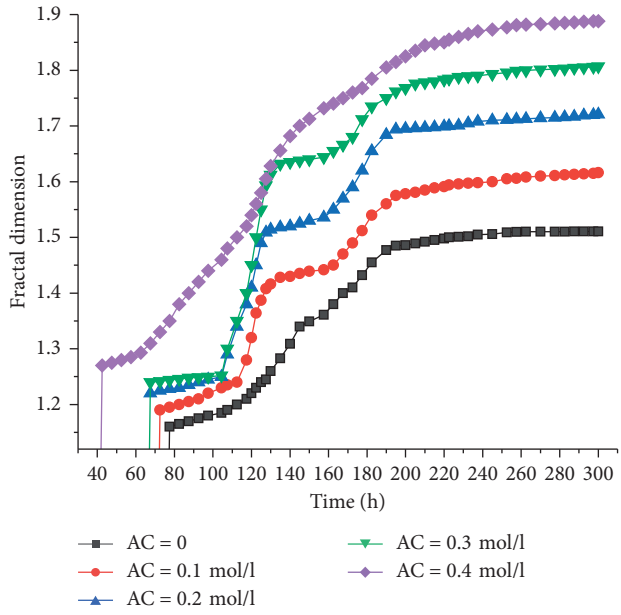


FIGURE 5: Drying time variations: fractal dimension of cracks in contaminated samples with different acid concentrations.

stage. When the acid concentration is greater than 0.4 mol/L, Stages I and III disappear with only steady crack development from the beginning to the end of the test.

*3.3. Stage I: Initial Cracking Stage.* In Stage I, as the water content decreases, a single crack first appears on the soil surface which is followed by further extension and development of the crack. With time, a network of primary cracks is formed by joining adjacent cracks due to the development of suction in the soil.

*3.4. Stage II: Crack Development Stage.* After the formation of the primary crack network, new cracks, which are referred to as subcracks, begin to branch out from the primary cracks with some growing perpendicular to the main cracks. Some subcracks subdivide the primary block formed by the primary cracks into more secondary networks until they intersect with the adjacent primary crack perpendicularly which will stop them from growing further. In some blocks formed by the secondary subcracks with large areas, it is possible to further develop branch cracks on the subcracks, thus leading to a complete secondary crack network.

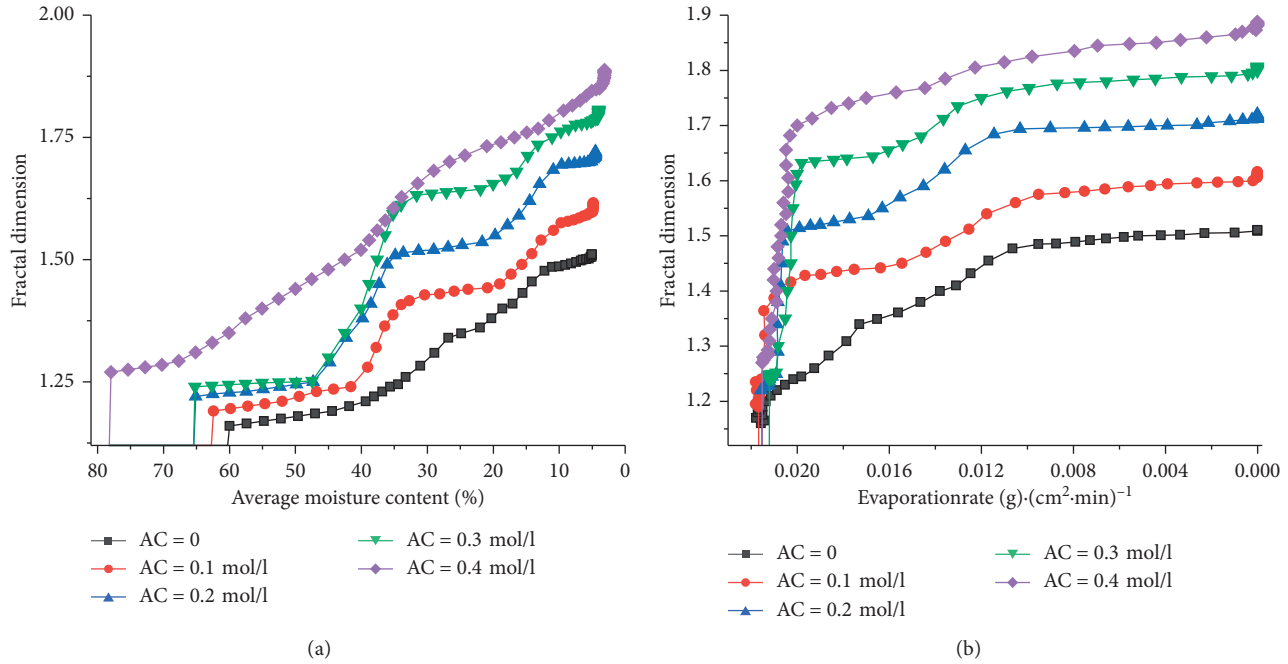


Figure 6: Fractal dimension variations of cracks in contaminated samples: (a) fractal dimension of cracks vs. average moisture content; (b) fractal dimension of cracks vs. evaporation rate.

*3.5. Stage III: Crack Stabilization Stage.* After the steady state stage of the development of a secondary crack network, no new cracks appear on the soil surface even though the evaporation continues. As drying continues, the existing cracks gradually widen until they finally stabilize. There is almost no change in the morphology of the surface crack network except that the cracks become a little wider.

Figure 7 shows the critical water content for crack formation with different acid concentrations. Suction and tensile strength are two main parameters that control crack formation [20]. The introduction of acid mainly affects the tensile strength of the soil during shrinkage. The acid reacts with the mineral composition of the clay which affects its cohesion and tensile strength. Figure 8 shows that as the acid concentration increases, a large amount of clay minerals is chemically decomposed by the acid which cannot resist the tensile stress developed in the soil. This leads to an increase in the deformation of the soil particles, thus reducing the stability of the soil particle structure. The results show that acid contamination can significantly weaken the mechanical strength of clay.

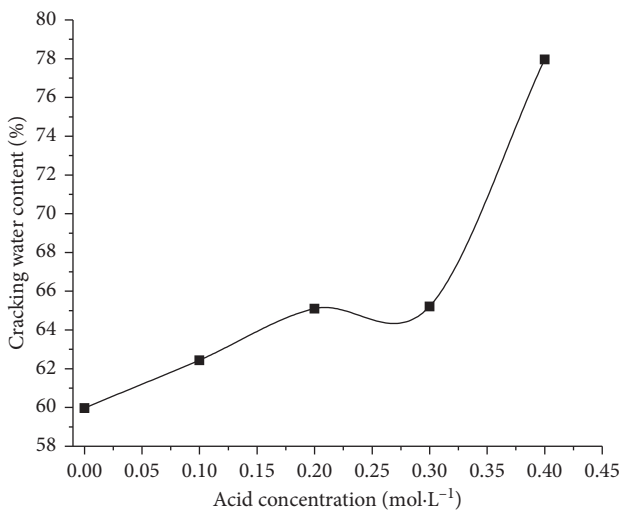


Figure 7: Critical moisture content with crack formation in contaminated samples with different acid concentration.

## 4. Discussion of Results

Clay minerals have high dispersibility, high hydrophilicity, strong adsorption, and ion exchange properties. Flat clay mineral particles are extremely small with a large specific surface area [21, 22]. They have strong physicochemical interaction with water and form the main components of the solid phase of clay. The interaction between clay minerals and HCl is the primary reason that the properties of acid contaminated clay are affected. The mass fraction of iron III oxide ($Fe_2O_3$) and aluminum oxide ($Al_2O_3$) in the clay minerals is relatively high, generally reaching up to 25%. When clay is contaminated with acid, a chemical reaction occurs with increase in the HCl concentration. The chemical process can be expressed by the following equation:

$$\begin{cases} Fe_2O_3 + 6HCl \longrightarrow 2FeCl_3 + 3H_2O \\ Al_2O_3 + 6HCl \longrightarrow 2AlCl_3 + 3H_2O \end{cases} \quad (8)$$

The clay in the studied area contains a large amount of calcium carbonate ($CaCO_3$) and magnesium carbonate ($MgCO_3$). When HCl is added to the clay, $CaCO_3$ and

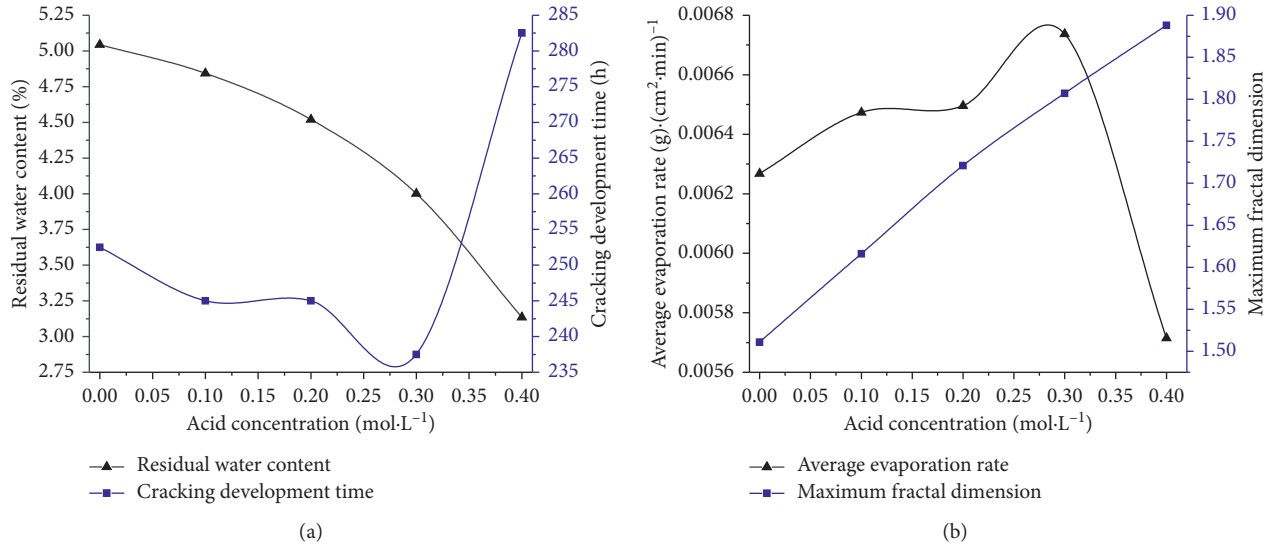


Figure 8: Residual water content, average evaporation rate, and maximum fractal dimension of cracks of contaminated samples with different acid concentrations: (a) residual water content, and (b) maximum fractal dimension.

$MgCO_3$ will be dissolved in the HCl solution due to an increase in the $H^+$ ions, resulting in $Ca^{2+}$ and $Mg^{2+}$ ions. The newly formed ions will react with the HCl solution according to the following equation:

$$\begin{cases} CaCO_3 + H^+ \longrightarrow Ca^{2+} + HCO_3^- \\ MgCO_3 + H^+ \longrightarrow Mg^{2+} + HCO_3^- \\ HCO_3^- + H^+ \longrightarrow H_2O + CO_2 \end{cases} \quad (9)$$

Figure 8(a) shows that as the concentration of the acid solution is increased, the residual water content of the sample is decreased, and the development time of the crack is also decreased. When the acid concentration is greater than 0.4 mol/L, the samples begin to crack at a water content of 78%. The chemical reaction of the clay minerals in the soil leads to a decrease in the hydrophilicity and adsorption properties of the soil. At the end of evaporation, the residual water content is the lowest with the longest crack development time.

As shown in Figure 8(b), the degree of cracking of the sample increases with a higher acid concentration and an increase in the average rate of evaporation. However, the average rate of evaporation of the soil is decreased when the acid concentration is greater than 0.3 mol/L. This is because when clay reacts chemically with the HCl, it corrodes the free oxides, carbonates, and minerals in the soil, thus causing disintegration of the aggregate structure of the soil. When the mass fraction of the clay is increased, the pore ratio and pore water content are increased accordingly. Meanwhile, with an increase in the evaporation time, the HCl corrodes the sesquioxides that act as a cement in the clay which then leads to a reduction in the cementation between the soil particles which in turn enhances crack development.

## 5. Conclusion

Acid contamination significantly changes the evaporation characteristics and development of desiccation cracks in soils. The evaporation characteristics of the soil samples contaminated with different acid concentrations can be divided into three stages: the steady rate of evaporation, deceleration of evaporation, and residual evaporation. With increases in the acid concentration, the critical water content, where there is a change in the rate of evaporation, decreases and the time to reach this water content increases. Surface crack development in soil with different acid concentrations can be divided into three stages: initial cracking, crack development, and crack stabilization. When the acid concentration is greater than 0.4 mol/L, the initial cracking and stabilization stages disappear, and only steady crack development is observed from the beginning to the end of the test. When the acid reacts chemically with the clay minerals in the soil, this results in a decrease in the hydrophilicity and adsorption properties of the soil which results in an increase in the water loss. There are other effects of acid on the evaporation characteristics of soil which should be investigated further. Field studies are also required to confirm the laboratory-scale results in this study.

## Data Availability

The data are available on request.

## Conflicts of Interest

The authors declare that they have no conflicts of interest

## Acknowledgments

The authors would like to acknowledge financial support from the Henan Key Scientific Research Projects of Colleges and Universities under Grant no. 21A410003.

## References

[1] W. Li, P. Ni, and Y. Yi, "Comparison of reactive magnesia, quick lime, and ordinary Portland cement for stabilization/solidification of heavy metal-contaminated soils," *Science of The Total Environment*, vol. 671, pp. 741–753, 2019.

[2] B. Yuan, L. Xiong, L. Zhai et al., "Transparent synthetic soil and its application in modeling of soil-structure interaction using optical system," *Frontiers in Earth Science*, vol. 7, Article ID 00276, 2019.

[3] B. Yuan, M. Sun, L. Xiong, Q. Luo, S. P. Pradhan, and H. Li, "Investigation of 3D deformation of transparent soil around a laterally loaded pile based on a hydraulic gradient model test," *Journal of Building Engineering*, vol. 28, Article ID 101024, 101024 pages, 2020.

[4] B. Yuan, M. Sun, Y. Wang, L. Zhai, Q. Luo, and X. Zhang, "Full 3D displacement measuring system for 3D displacement field of soil around a laterally loaded pile in transparent soil," *International Journal of Geomechanics*, vol. 19, no. 5, Article ID 04019028, 2019.

[5] R. García-Cervilla, A. Santos, A. Romero, and D. Lorenzo, "Remediation of soil contaminated by lindane wastes using alkaline activated persulfate: kinetic model," *Chemical Engineering Journal*, vol. 393, Article ID 124646, 124646 pages, 2020.

[6] G. J. Heij, W. de Vries, A. C. Posthumus, and G. M. J. Mohren, "4. Effects of air pollution and acid deposition on forests and forest soils," *Studies in Environmental Science*, vol. 46, pp. 97–137, 1991.

[7] H.-Q. Wang, Q. Zhao, D.-H. Zeng, Y.-L. Hu, and Z.-Y. Yu, "Remediation of a magnesium-contaminated soil by chemical amendments and leaching," *Land Degradation & Development*, vol. 26, no. 6, pp. 613–619, 2015.

[8] H. Wang, Y. Zeng, C. Guo et al., "Bacterial, archaeal, and fungal community responses to acid mine drainage-laden pollution in a rice paddy soil ecosystem," *Science of the Total Environment*, vol. 616-617, pp. 107–116, 2018.

[9] F. Zhang, M. Cheng, Z. Sun, L. Wang, Q. Zhou, and X. Huang, "Combined acid rain and lanthanum pollution and its potential ecological risk for nitrogen assimilation in soybean seedling roots," *Environmental Pollution*, vol. 231, pp. 524–532, 2017.

[10] B. Liao, Z. Guo, A. Probst, and J.-L. Probst, "Soil heavy metal contamination and acid deposition: experimental approach on two forest soils in Hunan, Southern China," *Geoderma*, vol. 127, no. 1-2, pp. 91–103, 2005.

[11] H. Peron, T. Hueckel, L. Laloui, and L. B. Hu, "Fundamentals of desiccation cracking of fine-grained soils: experimental characterisation and mechanisms identification," *Canadian Geotechnical Journal*, vol. 46, no. 10, pp. 1177–1201, 2009.

[12] P. V. Divya, B. V. S. Viswanadham, and J. P. Gourc, "Influence of geomembrane on the deformation behaviour of clay-based landfill covers," *Geotextiles and Geomembranes*, vol. 34, pp. 158–171, 2012.

[13] S. Rajesh and B. V. S. Viswanadham, "Evaluation of geogrid as a reinforcement layer in clay based engineered barriers," *Applied Clay Science*, vol. 46, no. 2, pp. 153–165, 2009.

[14] H. Rahardjo, T. H. Ong, R. B. Rezaur, and E. C. Leong, "Factors controlling instability of homogeneous soil slopes under rainfall," *Journal of Geotechnical and Geoenvironmental Engineering*, vol. 133, no. 12, pp. 1532–1543, 2007.

[15] L. Zeng, J. Liu, J.-H. Zhang, H.-B. Bian, and W.-H. Lu, "Effect of colluvial soil slope fracture's anisotropy characteristics on rainwater infiltration process," *Advances in Civil Engineering*, vol. 2018, Article ID 7351628, 11 pages, 2018.

[16] P. D. Hallett and T. A. Newson, "Describing soil crack formation using elastic-plastic fracture mechanics," *European Journal of Soil Science*, vol. 56, no. 1, pp. 31–38, 2005.

[17] K. F. DeCarlo and N. Shokri, "Effects of substrate on cracking patterns and dynamics in desiccating clay layers," *Water Resources Research*, vol. 50, no. 4, pp. 3039–3051, 2014.

[18] H. U. Levatti, P. C. Prat, A. Ledesma, A. Cuadrado, and J. A. Cordero, "Experimental analysis of 3D cracking in drying soils using ground-penetrating radar," *Geotechnical Testing Journal*, vol. 40, no. 2, Article ID GTJ20160066, 2017.

[19] C. Wang, Z.-Y. Zhang, Y. Liu, and S.-M. Fan, "Geometric and fractal analysis of dynamic cracking patterns subjected to wetting-drying cycles," *Soil and Tillage Research*, vol. 170, pp. 1–13, 2017.

[20] J. Li, C. Tang, D. Wang, X. Pei, and B. Shi, "Effect of discrete fibre reinforcement on soil tensile strength," *Journal of Rock Mechanics and Geotechnical Engineering*, vol. 6, no. 2, pp. 133–137, 2014.

[21] R. Mukhopadhyay, D. Bhaduri, B. Sarkar et al., "Clay-polymer nanocomposites: progress and challenges for use in sustainable water treatment," *Journal of Hazardous Materials*, vol. 383, Article ID 121125, 2020.

[22] J. Hou, H. Bossuyt, S. Degryze, and K. Denef, "A history of research on the link between (micro) aggregates, soil biota, and soil organic matter dynamics," *Soil and Tillage Research*, vol. 79, no. 1, pp. 7–31, 2004.